

Many-body and model-potential calculations of low-energy photoionization parameters for francium

A. Derevianko and W. R. Johnson

Department of Physics, Notre Dame University, Notre Dame, IN 46556

H. R. Sadeghpour

Institute for Theoretical Atomic and Molecular Physics

Harvard-Smithsonian Center for Astrophysics, Cambridge, MA 02138

(August 6, 2018)

The photoionization cross section σ , spin-polarization parameters P and Q , and the angular-distribution asymmetry parameter β are calculated for the $7s$ state of francium for photon energies below 10 eV. Two distinct calculations are presented, one based on many-body perturbation theory and another based on the model potential method. Although predictions of the two calculations are similar, the detailed energy dependence of the photoionization parameters from the two calculations differ. From the theoretical p -wave phase shifts, we infer quantum defects for $p_{1/2}$ and $p_{3/2}$ Rydberg series, permitting us to calculate positions of experimentally unknown p states in francium.

31.15.Md, 32.80.Fb, 33.60.-q

I. INTRODUCTION

Remarkable progress has been made recently in determining energies and lifetimes of low-lying states of the heaviest alkali-metal atom francium [1], motivated in part by the enhancement of parity non-conserving (PNC) effects in francium compared with other alkali-metal atoms. This experimental work has been accompanied by theoretical studies of properties of the francium atom [2,3], concerned mostly with energies and hyperfine constants of the ground and low-lying excited states or transitions between such states.

In this work, we present two calculations of photoionization of francium for photon energies below 10 eV; the first is an *ab-initio* many-body calculation and the second is a model potential (MP) calculation. Experiments on photoionization of francium are planned for the Advanced Light Source at Berkeley. [4]

Ab-initio calculations of photoionization in alkali-metal atoms have proved to be a formidable challenge. Photoionization calculations in cesium based on the Dirac or Breit-Pauli equations [5–7] accounted for the spin-orbit interaction, but not for shielding of the dipole operator by the core electrons or for core-polarization effects; whereas, relativistic calculations that included corrections from many-body perturbation theory (MBPT) at the level of the random-phase-approximation (RPA) [8,9] accounted for the spin-orbit effects and for core

shielding, but not core polarization. Predictions from these many-body calculations were in poor agreement with measurements of the Fano spin-polarization parameter P by Heinzmann *et al.* [10], of the spin-polarization parameter Q by Lubell *et al.* [11], and with the measurement of the angular-distribution asymmetry parameter β by Yin and Elliott [12]. The first quantitatively successful many-body calculation of photoionization of cesium was a relativistic many-body calculation that included both core polarization and core shielding corrections [13]; that method is applied to low-energy photoionization of francium in the present paper.

Although successful many-body calculations of photoionization of heavy alkali-metal atoms are of recent vintage, nearly three decades ago, a number of increasingly sophisticated and successful model potential calculations of the photoionization of cesium appeared [14–17], culminating with that of Norcross [18]. The latter calculation, which included the spin-orbit interaction, long-range polarization potentials, and shielding corrections to the dipole operator, gave quantitatively correct values for all of the measured photoionization parameters in cesium. A model potential similar to the one used in [18] was developed recently [3] to study transitions in francium and is used here to study low-energy photoionization in francium.

Below, we sketch the important features of the theoretical methods. The photoionization cross sections for Fr $7s$ are calculated in Section II.B in both methods and are compared against one another. In Section II.E, we give results for the spin-polarization parameters and the angular distribution asymmetry parameter. Section III concludes our discussion of the francium photoionization.

II. THEORETICAL ANALYSIS & DISCUSSION

A. Many-Body Perturbation Theory

We start our many-body analysis from the Dirac-Hartree-Fock (DHF) V_{N-1} approximation, in which the DHF equations are solved self-consistently for core orbitals, and the valence orbitals are determined subsequently in the field of the “frozen core”. The total phase shift $\tilde{\delta}_\kappa$ for a continuum state with angular quantum

number κ in the field of the core is a sum of rapidly varying Coulomb phase shift δ_κ^C and the short-range shift δ_κ . The short-range DHF phase-shifts for $p_{1/2}$ and $p_{3/2}$ continuum wave functions are shown in Fig. 1. The $p_{3/2}$ wave function lags in phase compared to the $p_{1/2}$ wave function owing to the spin-orbit interaction, which is attractive for $p_{1/2}$ states and repulsive for $p_{3/2}$ states. The DHF approximation typically underestimates removal energies of bound electrons in heavy atoms such as francium by about 10%; similar accuracy is expected for phase shifts. To improve this level of accuracy one must take into account higher-order MBPT corrections.

The clear advantage of the V_{N-1} approximation stems from the fact that one-body contributions to the residual Coulomb interaction vanish. This leads to a significant reduction in the number of terms in the order-by-order MBPT expansion. In particular, first-order corrections to the energy (or the phase shift) vanish and the perturbation expansion starts in second-order.

The leading correlation contribution to the energy is the expectation value of the second-order self-energy operator $\Sigma^{(2)}$, given diagrammatically by the Brueckner-Goldstone diagrams of Fig. 2. Solutions to the Dirac equation including the V_{N-1} potential and the self-energy operator are called Brueckner orbitals (BO). The non-local self-energy operator Σ , in the limit of large r , describes the interaction of an electron with the induced electric moments of the core,

$$\Sigma(r, r', \epsilon) \rightarrow -\frac{\alpha_d}{2r^4} \delta(r - r'), \quad (1)$$

where α_d is the dipole polarizability of the core. We determine second-order correction to the phase shift perturbatively as

$$\delta_\kappa^{(2)} = -\sin^{-1}(\pi \langle u_{\epsilon\kappa} | \Sigma^{(2)} | u_{\epsilon\kappa} \rangle). \quad (2)$$

Here, $u_{\epsilon\kappa}$ is a continuum DHF wave function normalized on the energy scale. The resulting DHF+BO phase shifts are presented in Fig. 1. The attractive polarization potential draws in the nodes of the wave function, resulting in larger phase shifts. The change in the phase shift is approximately the same for both $p_{3/2}$ and $p_{1/2}$ continuum states, demonstrating that the self-energy correction is mainly due to the accumulation of phase outside of the core.

B. Model Potential

The parametric model potential used in this work has the form [21]

$$V_\ell^{(j)}(r) = \frac{Z_{\ell j}(r)}{r} - \frac{\alpha_d}{2r^4} [1 - e^{-(r/r_c^{(j)})^6}], \quad (3)$$

where α_d is the static dipole polarizability of the Fr^+ ionic core and the effective radial charge $Z_{\ell j}(r)$ is given by

$$Z_{\ell j}(r) = 1 + (z - 1)e^{-a_1^{(j)}r} + r(a_3^{(j)} + a_4^{(j)}r)e^{-a_2^{(j)}r}. \quad (4)$$

The angular momentum-dependent parameters, $a_i^{(j)}$, $i = 1, \dots, 4$ and the cut-off radius $r_c^{(j)}$ are obtained through a non-linear fit to one-electron Rydberg energy levels in francium [1,2,19]. Because the spin-orbit effects are appreciable for heavy alkali metals, two separate nonlinear fits; one for each fine-structure series, $j_+ = \ell + \frac{1}{2}$ and $j_- = \ell - \frac{1}{2}$ were performed. The static dipole polarizability was obtained from an extrapolation of the known core polarizabilities for the other alkali metals as $\alpha_d(0) = 23.2$ a.u. [3]. We note that an *ab initio* value for the francium core polarizability is now available [2].

A comparison of short-range phase shifts calculated in the model-potential method and the MBPT is presented in Fig. 3. We find reasonable agreement between the two methods. The MP continuum wavefunctions are slightly lagging in phase compared to many-body wavefunctions. Such phase differences result in Cooper minima being shifted to higher photoelectron momentum in the model-potential calculation.

C. Quantum defects

In quantum defect (QD) theory [20], the energy levels of the valence electron are described by a hydrogen-like Rydberg-Ritz formula

$$\epsilon_{n\kappa} = -\frac{1}{2(n - \mu_\kappa)^2} \quad (5)$$

in terms of a quantum defect μ_κ , which is represented as an expansion in powers of energy with constant coefficients $\mu_\kappa^{(i)}$

$$\mu_\kappa = \mu_\kappa^{(0)} + \mu_\kappa^{(1)}\epsilon_{n\kappa} + \mu_\kappa^{(2)}(\epsilon_{n\kappa})^2 + \dots \quad (6)$$

The Rydberg-Ritz formula provides an accurate fitting expression for the bound spectrum of alkalis. The QD $\mu_\kappa^{(0)}$ is related to threshold value of the phase shift as $\mu_\kappa^{(0)} = \delta_\kappa/\pi + \text{integer}$. The QD's for Fr p states are not known, since the relevant Rydberg series have not been observed experimentally. We use our *ab-initio* threshold phase shifts together with experimentally known energies for $7p$ and $8p$ states to predict QD's; thereby approximating the entire Rydberg spectrum of Fr p states. The predicted quantum defects are given in Table I. We assigned an error bar of 0.5% to the threshold phase shift, based on the accuracy of an application of the many-body formalism employed here to the case of Cs [13].

In Table I, we also present the MP values of quantum-defects obtained by fitting Rydberg series calculated with the potential in Eq. 3. We find generally good agreement for the leading order quantum-defect $\mu_\kappa^{(0)}$, estimated in the two methods. Higher-order QD parameters, $\mu_\kappa^{(1)}$ and $\mu_\kappa^{(2)}$, calculated in the two methods do not agree well.

This is due to the sensitivity of these parameters to the value of $\mu_\kappa^{(0)}$. The values for $\mu_\kappa^{(0)}$ obtained by fitting to the MP-calculated np levels agree to four significant digits with the values, for $\mu_\kappa^{(0)}$, extracted from the threshold phase shifts in Fig. 3.

Using the calculated quantum defects, we predict energy levels for the lowest few np states. Table II lists these energies and compares them with the present MP calculation and with a recent MBPT single-double (SD) calculation [22]. The accuracy of our many-body calculation was estimated by exercising upper and lower bounds on $\mu_\kappa^{(0)}$, and a consistent determination of $\mu_\kappa^{(1)}$ and $\mu_\kappa^{(2)}$ to fit $7p$ and $8p$ energies. MBPT results are in reasonable agreement with the MP calculations and SD predictions for these levels.

D. Cross-section

The total cross-section for photoionization of the valence electron v is the sum of partial cross-sections

$$\sigma = \sum_{\kappa} \sigma_{\kappa} = \frac{4\pi^2\alpha}{3}\omega \sum_{\kappa} |D_{\kappa}|^2, \quad (7)$$

where ω is the photon energy. The dipole transition amplitude for an ionization channel $v \rightarrow \epsilon\kappa$ is defined as

$$D_{\kappa} = i^{-l+1} e^{i\delta_{\kappa}} \langle u_{\epsilon\kappa} | \mathbf{r} | u_v \rangle, \quad (8)$$

where u_v is the valence wave function and where the continuum wave function $u_{\epsilon\kappa}$ is normalized on the energy scale. Here we have two ionization channels $7s \rightarrow \epsilon p_{1/2}$, with $\kappa = 1$ and $7s \rightarrow \epsilon p_{3/2}$, with $\kappa = -2$. The DHF results for the total cross-section are shown with dashed lines in Fig. 4. Since the DHF potential is non-local, the resulting amplitudes depend on the gauge of the electromagnetic field. The difference between length- and velocity-form values is especially noticeable in the near-threshold region.

Second-order corrections, and the associated all-order sequence of random-phase approximation (RPA) diagrams, account for the shielding of the external field by the core electrons. Explicit expressions for the second-order MBPT corrections can be found, for example, in Ref. [25]. Already in second order, the dipole operator with RPA corrections reduces at large r to an effective one-particle operator

$$\mathbf{r}_{\text{eff}} = \mathbf{r} \left(1 - \frac{\alpha_d(\omega)}{r^3} \right), \quad (9)$$

where $\alpha_d(\omega)$ is a *dynamic* polarizability of the core. The first term is associated with the applied electric field and the second with the field of the induced dipole moment of the atomic core; the valence electron responds to a sum of these two fields. We note that the induced field may become strong and reverse the direction of the total field.

The RPA cross-section is presented with a thin solid line in Fig. 4. In contrast to DHF amplitudes, the RPA amplitudes are gauge-independent. Furthermore, we note the sudden upturn in the RPA cross-section for the photoelectron momenta $p \approx 0.7$ a.u. associated with a $J = 1$ core excitation resonance. To predict the position of this resonance, we calculate the dynamic polarizability of Fr^+ within the framework of relativistic RPA, discussed in [24]. The energy of the first resonance is at $\omega_r = 0.4024$ a.u.. Using the DHF value of $7s$ threshold, 0.1311 a.u., we expect the first core excitation resonance to appear at $p \approx 0.74$ a.u.. The dynamic polarizability of Fr core $\alpha_d(\omega)$ from this RPA calculation is plotted as a function of electron momentum p in Fig. 5.

To account for *core-polarization* corrections to the DHF wave function, discussed in the introduction, we evaluate the second-order corrections to the DHF wave functions of the valence electron due to the self-energy operator $\Sigma^{(2)}$

$$u_v^{(2)} = \sum_{i \neq v} \frac{\Sigma_{iv}^{(2)}}{\epsilon_v - \epsilon_i} u_i. \quad (10)$$

The resulting orbital $u_v + u_v^{(2)}$ is the perturbative approximation to the valence-state Brueckner orbitals (BO). Approximate Brueckner orbitals for a continuum state ($\epsilon\kappa$) are found by solving the inhomogeneous Dirac equation

$$(h + V_{N-1} - \epsilon) w_{\epsilon\kappa} = \left(-\pi \sin \delta_{\kappa} - \Sigma^{(2)} \right) u_{\epsilon\kappa} \quad (11)$$

normalized on the energy scale, where δ_{κ} is given in Eq. (2). Brueckner orbitals for the $7s$ valence state and a $p_{1/2}$ continuum state are compared with unperturbed DHF orbitals in Fig. 6.

The BO corrections contribute to transition amplitudes starting from third order. Together with the RPA corrections, they provide the most important third-order contributions for bound-bound transitions, as discussed in [25]. In the present approach, we modify the conventional RPA scheme by replacing the valence and continuum wave functions by the approximate Brueckner orbitals described above (RPA \oplus BO). Such a modification accounts for the important second- and third-order correlation corrections and for a subset of fourth-order contributions to transition amplitudes. We note that this fourth-order subset brings the photoionization parameters in cesium into good agreement with available experimental data; therefore, we believe that this approach will provide reliable predictions for francium. The resulting cross section is shown with a heavy solid line in Fig. 4, and decomposed into partial cross-sections in Fig. 7. Calculations using length and velocity forms of transition operator lead to slightly different result in the modified RPA \oplus BO scheme; we present the final result in the length form only. Both photoionization channels exhibit Cooper minima; $\sigma_{p_{1/2}}$ vanishes at $p \approx 0.1$ a.u. and $\sigma_{p_{3/2}}$ vanishes at $p \approx 0.5$ a.u.. Combining the two

partial cross sections, leads to a broad minimum in the total cross-section slightly below $p = 0.45$ a.u.. The total cross section in Fig. 7 is not very sensitive to the positions of Cooper minima in the $p_{1/2}$ and $p_{3/2}$ channels. Conversely, the spin-polarization and angular distribution measurements, discussed in the following section, provide information sensitive to fine details of individual transition amplitudes.

Fig. 8 examines the total photoionization cross sections for francium, calculated in the two methods. The label "static" refers to the set of MP results with the core static dipole polarizability in Eq. 9. The shielding of the electron dipole operator is truncated in the MP calculations by introducing a cut-off term, similar to the exponential term in the one-electron potential in Eq. 3. The threshold cross sections in the $p_{1/2}$ and $p_{3/2}$ channels (not shown here) are, respectively, 1.74 and 0.02 Mb. Cooper minima appear in both channels at approximately, $p \approx 0.15$ a.u. and $p \approx 0.75$ a.u. and the maximum cross section in the $p_{1/2}$ channel is $\sigma_{p_{1/2}}(\text{max}) \approx 0.2$ Mb. The Cooper minimum in the $p_{3/2}$ photoelectron cross section calculated in the MP method with the static core dipole polarizability, occurs approximately where the first core resonance in Fig. 5 becomes excited. By including the dynamic core polarizability $\alpha_d(\omega)$ in the MP calculations, the curve labeled as "dynamic" in Fig. 8 is obtained. The Cooper minima are moved to lower photoelectron momenta, resulting in a shallow minimum in the total cross section near $p \approx 0.5$ a.u.

The comparison in Fig. 8 indicates that the cross sections calculated in the MP method are in general larger than the MBPT cross sections. The "MP dynamic" and the MBPT cross sections both rise for the photoelectron momenta $p > 0.5$ a.u. to meet the first core-excited resonance near $p \sim 0.75$ a.u.

E. Polarization parameters

Fano [10] proposed a measurement of spin polarization P of photoelectrons emitted from unpolarized Cs atoms illuminated by circularly polarized photons. The total spin polarization is expressed in terms of $p_{1/2}$ and $p_{3/2}$ transition amplitudes as [23]¹

$$P = \frac{5|D_{3/2}|^2 - 2|D_{1/2}|^2 + 4\sqrt{2}\Re[D_{1/2}D_{3/2}^*]}{6(|D_{3/2}|^2 + |D_{1/2}|^2)}. \quad (12)$$

The result of our RPA \oplus BO calculation of the spin-polarization parameter P is presented in Fig. 9, where

¹ There is a phase difference in the $D_{1/2}D_{3/2}^*$ interference term in Eqs. 12,14 and the corresponding equations in Ref. [23], caused by the unconventional definition of reduced matrix elements used in that work.

it is seen that the polarization reaches 100% at momentum $p \approx 0.3$ a.u. The model-potential results for P are also given in Fig. 9 and compare well with the RPA \oplus BO calculation in Fig. 9. Maximum spin polarization in the MP method occurs at $p \approx 0.35$ a.u. The calculations with the static and dynamic core polarizabilities in Eq. 9 are similar and differ only after the maximum is reached.

Lubell and Raith [11] measured a different spin-polarization parameter Q obtained from photoionization of polarized Cs atoms by a circularly polarized light. In the Lubell-Raith setup, the $p_{3/2}$ channel can be accessed individually, for example, by photoionization with left-circularly polarized light of the $7s$, electron prepared in the $m_s = +\frac{1}{2}$ substate. Combining the partial cross section $\sigma_{p_{3/2}}$ thereby obtained with the total cross-section, permits one to deduce the partial cross-section for the $p_{1/2}$ channel. The Lubell-Raith parameter Q is defined as the ratio of the difference to the total of the photoabsorption intensities for two photon helicities

$$Q = \frac{I_+ - I_-}{I_+ + I_-} = \frac{|D_{3/2}|^2 - 2|D_{1/2}|^2}{2(|D_{3/2}|^2 + |D_{1/2}|^2)}. \quad (13)$$

The limiting values for the Lubell-Raith parameter are $-1 \leq Q \leq \frac{1}{2}$. We stress that a measurement of Q or of the (phase-insensitive) parameter P , together with a measurement of the total cross-section permits one to obtain information about *absolute* values of transition amplitudes. A further measurement of the phase-sensitive angular-distribution parameter β [23],

$$\beta = \frac{|D_{3/2}|^2 - 2\sqrt{2}\Re[D_{1/2}D_{3/2}^*]}{|D_{3/2}|^2 + |D_{1/2}|^2}, \quad (14)$$

would permit one to determine the relative phase between the $p_{3/2}$ and $p_{1/2}$ continuum amplitudes and would constitute an essentially *complete* description of the photoionization process. The many-body result for β is shown in Fig. 9. The differential cross section is proportional to $1 - \frac{1}{2}\beta P_2(\cos\theta)$.

The MP results for Q and the asymmetry parameter β are given also in Fig. 9. The comparison between MP and MBPT results is generally favorable; the results with the core dynamics polarizability in Eq. 9 are in better qualitative agreement with the MBPT calculations. We note that near $p \approx 0.45$ a.u., the photoelectron has the propensity to be ionized perpendicular to the photon polarization axis and near $p \approx 0.6$ a.u., the photoelectron is preferentially ejected in the $j = \frac{1}{2}$ channel, where $Q \rightarrow -1$. A similar situation is evident from MBPT results at $p \approx 0.5$. The other limiting value is reached near threshold, where $\sigma_{p_{1/2}} \rightarrow 0$.

III. CONCLUSION

We have calculated the photoionization cross sections of the ground-state francium. Both many-body and

model-potential approaches were employed to obtain the cross sections, quantum defects, spin-polarization parameters and photoelectron asymmetry parameter. We find Cooper minima in both $p_{1/2}$ and $p_{3/2}$ channels. The comparison between the MBPT and MP results are satisfactory. The Cooper minima predicted in the MP calculations are at higher photoelectron energies than those calculated in the MBPT method. The origin of this difference can be traced to the shielding of the valence-electron dipole by the core electrons. The induced dipole moment of the core manifests itself as a dynamic polarizability term. Upon replacing the static core polarizability with the dynamic polarizability, better quantitative agreement with the MBPT results is observed. We predict the energy-dependence of the photoelectron spin-polarization and asymmetry parameters which we hope will stimulate further experimental work in francium.

ACKNOWLEDGMENTS

The work of AD and WRJ was supported in part by NSF Grant No. PHY 99-70666. HRS is supported by a grant by NSF to the Institute for Theoretical Atomic and Molecular Physics. The authors owe a debt of gratitude to Harvey Gould for describing his proposed measurement of σ and Q for francium.

-
- [1] J. E. Simsarian, W. Z. Zhao, L. A. Orozco and G. D. Sprouse, Phys. Rev. A **59**, 195 (1999); G. D. Sprouse, L. A. Orozco, J. E. Simsarian and W. Z. Zhao, Nucl. Phys. A **630**, 316C (1998); J. E. Simsarian, L. A. Orozco, G. D. Sprouse and W. Z. Zhao, Phys. Rev. A **57**, 2448 (1998); W. Z. Zhao, J. E. Simsarian, L. A. Orozco, W. Shi and G. D. Sprouse, Phys. Rev. Lett. **78**, 4169 (1998); G. D. Sprouse, L. A. Orozco, J. E. Simsarian, W. Shi and W. Z. Zhao, Optics Lett. **21**, 1939 (1996).
 - [2] A. Derevianko, W. R. Johnson, M. S. Safronova and J. F. Babb, Phys. Rev. Lett. **82**, 3589 (1999); T. M. R. Byrnes, V. A. Dzuba, V. V. Flambaum and D. W. Murray, Phys. Rev. A **59**, 3082 (1999); W. A. Van Wijngaarden and J. Xia, J. Quant. Spectrosc. & Radiat. Transfer **61**, 557 (1999); E. Biemont, P. Quinet and V. Van Renterghem, J. Phys. B **31** 5301 (1998); A. Owusu, R. W. Dougherty, G. Gowri, T. P. Das and J. Andriessen; Phys. Rev. A **56**, 305 (1997). W. R. Johnson, Z. W. Liu and J. Sapirstein, At. Data Nucl. Data Tables **64**, 279 (1996); V. A. Dzuba, V. V. Flambaum, and O. P. Sushkov, Phys. Rev. A **51**, 3454 (1995). E. Eliav, U. Kaldor and Y. Ishikawa, Phys. Rev. A **50**, 1121 (1994).
 - [3] M. Marinescu, D. Vrinceanu, and H. R. Sadeghpour, Phys. Rev. A **58**, R4259 (1998).
 - [4] Harvey Gould, private communication.
 - [5] J. J. Chang and H. P. Kelly, Phys. Rev. A **5**, 1713 (1972).
 - [6] W. Ong and S. T. Manson, Phys. Rev. A **20**, 2364 (1979).
 - [7] K.-N. Huang and A. F. Starace, Phys. Rev. A **19**, 2335 (1979).
 - [8] W. R. Johnson and G. Soff, Phys. Rev. Lett. **50**, 1361 (1983).
 - [9] M. G. J. Fink and W. R. Johnson, Phys. Rev. A **34**, 3754 (1986).
 - [10] U. Fano, Phys. Rev. **178**, 131 (1969); U. Heinzmann, J. Kessler and J. Lorenz, Z. Phys. A **240**, 42 (1970).
 - [11] M. S. Lubell and W. Raith, Phys. Rev. Lett. **23**, 211 (1969); G. Baum, M. S. Lubell and W. Raith, Phys. Rev. Lett. **25**, 267 (1970).
 - [12] Y. Y. Yin and D. S. Elliott, Phys. Rev. A **46**, 1339 (1992).
 - [13] W. R. Johnson, Indian J. Phys. **71B**, 263 (1997).
 - [14] S. Hameed, A. Hertenberg, and M. G. James, J. Phys. B **1**, 822 (1968); S. Hameed, Phys. Rev. **179**, 16 (1969).
 - [15] I. L. Beigman, L. A. Vainshtein, and V. P. Shevelko, Opt. Spectrosc. **28**, 229 (1970).
 - [16] J. C. Weisheit and A. Dalgarno, Phys. Rev. Lett. **27**, 701 (1971).
 - [17] J. C. Weisheit, Phys. Rev. A **5**, 1621 (1972).
 - [18] D. W. Norcross, Phys. Rev. A **7**, 606 (1973).
 - [19] E. Arnold *et al.*, J. Phys. B **22**, L391(1989); J. Phys. B **25**, 3511(1990); J. Bauche *et al.*, J. Phys. B **19**, L593(1986); H. T. Duong *et al.*, Europhys. Lett. **3**, 175(1987); S. V. Andreev, V. S. Letokhov and V. I. Mishin, Phys. Rev. Lett. **59**, 1274(1987); J. Opt. Soc. Am. B **5**, 2190(1988); S. Liberman *et al.*, C. R. Acad. Sci. Paris **268B**, 253(1987).

- [20] M. J. Seaton, Mon. Not. R. Astron. Soc. **118**, 504 (1958); U. Fano, Phys. Rev. A **2**, 353 (1970).
- [21] M. Marinescu, R. H. Sadeghpour, and A. Dalgarno, Phys. Rev. A **49**, 982 (1994); C. H. Greene, Phys. Rev. A **42**, 1405(1990).
- [22] M. S. Safronova, W. R. Johnson, and A. Derevianko (submitted to Phys. Rev. A, 1999).
- [23] K.-N. Huang, W. R. Johnson, and K. T. Cheng, At. Data Nucl. Data Tables **26**, 33 (1981).
- [24] A. Dalgarno and W. D. Davidson, Adv. At. Mol. Phys. **2**, 1 (1966); D. Kolb, W. R. Johnson, and P. Shorer, Phys. Rev. A **26**, 19 (1982); W. R. Johnson, D. Kolb, and K.-N. Huang, At. Data Nucl. Data Tables **28**, 333 (1983).
- [25] W. R. Johnson, Z. W. Liu, and J. Sapirstein, At. Data Nucl. Data Tables **64**, 280 (1996).

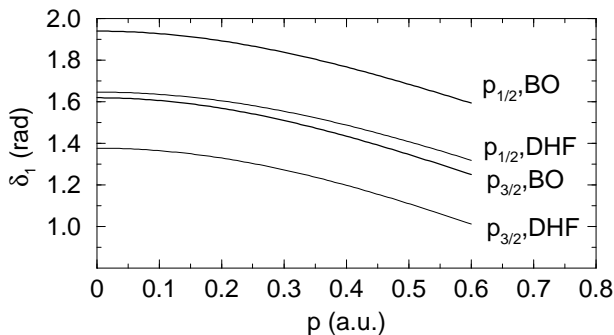


FIG. 1. Short-range phase shifts for p continuum in Fr calculated in Dirac-Hartree-Fock (DHF) approximation and including self-energy correction (BO).

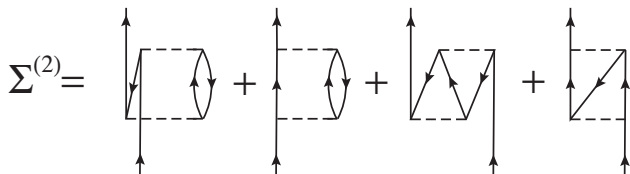


FIG. 2. The second-order self-energy operator.

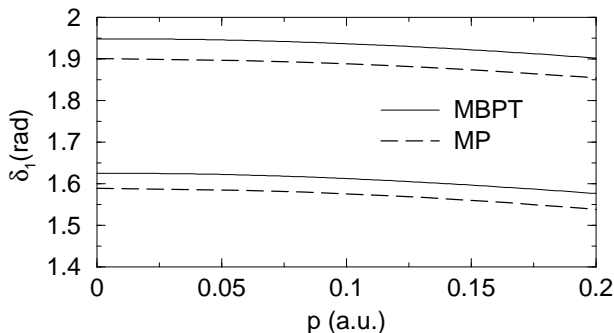


FIG. 3. Comparison of short-range phase shifts obtained in model potential and many-body methods. Upper two curves represent $p_{1/2}$ -phase shifts, and two lower curves represent those for $p_{3/2}$ continuum.

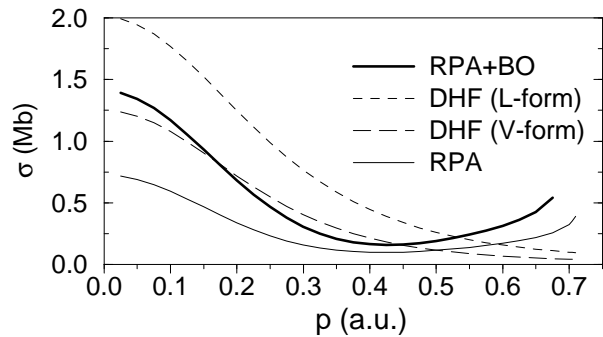


FIG. 4. Total photoionization cross-sections for Fr $7s$ state, calculated in various many-body approximations.

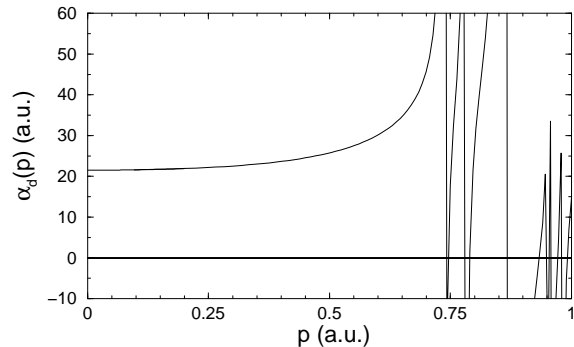


FIG. 5. RRPA dynamic polarizability of Fr^+ as a function of photoelectron momentum, calculated with the $7s$ DHF threshold, 0.13107 a.u..

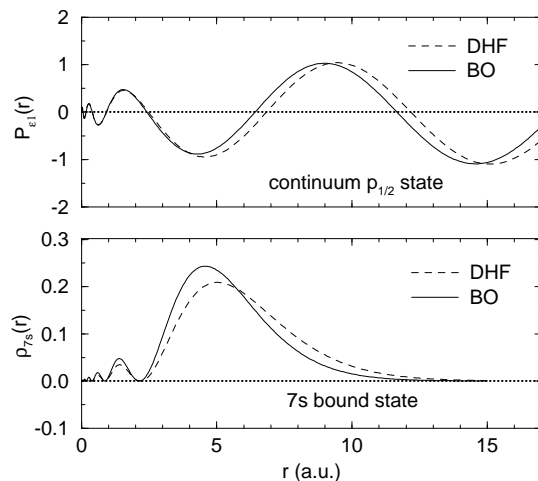


FIG. 6. Brueckner (BO) and DHF orbitals. Upper panel: large component of continuum wave function; Lower panel: radial density.

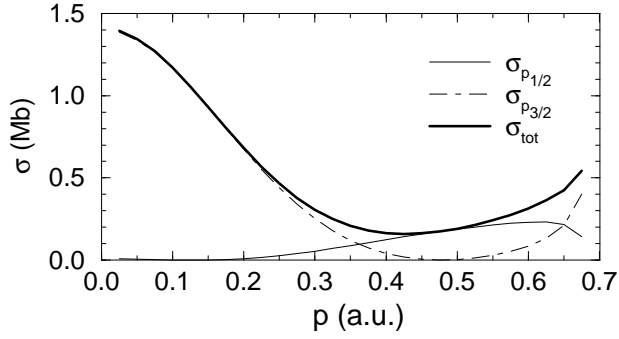


FIG. 7. Partial and total cross-sections for Fr $7s$ calculated in the RPA \oplus BO many-body approach.

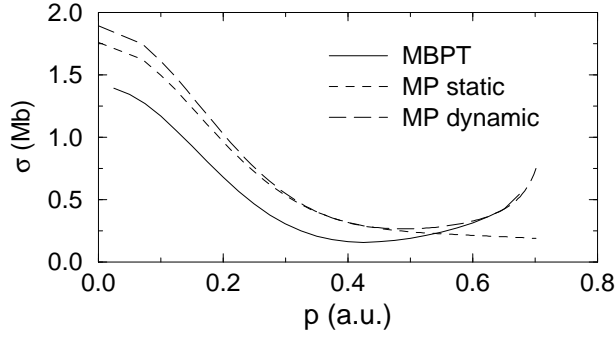


FIG. 8. Comparison of Fr $7s$ photoionization cross sections calculated with the MBPT and the MP methods. The curves labeled as "static" and "dynamic" refer, respectively, to the calculations with static and dynamic core polarizabilities in Eq. 9.

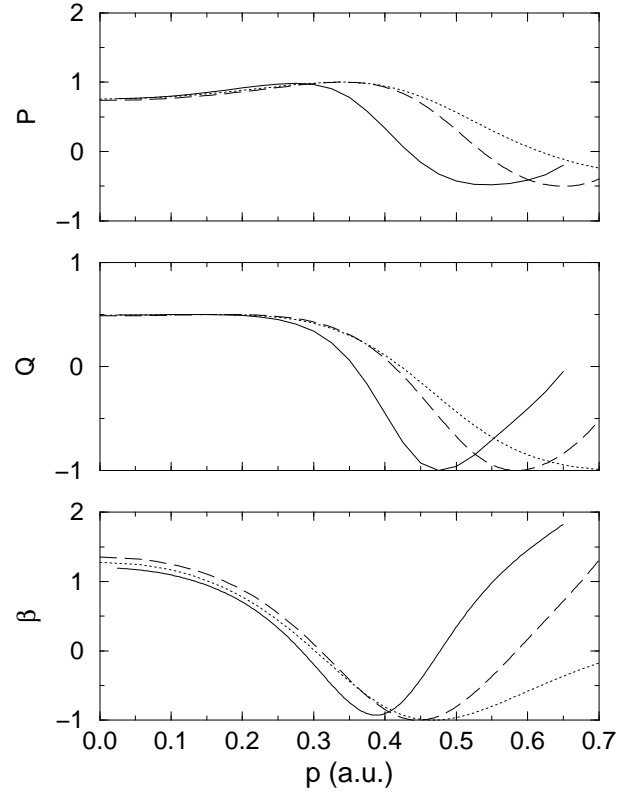


FIG. 9. Fano P and Lubell-Raith Q spin-polarization parameters, and dipole asymmetry parameter β , calculated in the RPA \oplus BO (solid line) and MP approach. The long-dashed curve represents the MP results using the RRPA dynamic polarizability in the transition operator, and dotted curve — static polarizability instead.

TABLE I. Predicted quantum-defect parameters

state	$\mu_{\kappa}^{(0)}$	$\mu_{\kappa}^{(1)}$	$\mu_{\kappa}^{(2)}$
MBPT			
$p_{1/2}$	4.620(3)	-0.3(1)	5.3(7)
$p_{3/2}$	4.517(3)	-0.5(1)	4.7(8)
Model Potential			
$p_{1/2}$	4.605	-0.79	1.61
$p_{3/2}$	4.505	-0.87	1.59

TABLE II. Predicted p levels of Fr in cm^{-1} .

state	Present Work		SD ^b [22]
	QDT+MBPT ^a	MP	
$9p_{1/2}$	5748(3)	5737	5738
$10p_{1/2}$	3800(2)	3790	3795
$11p_{1/2}$	2700(2)	2691	
$12p_{1/2}$	2016(1)	2011	
$9p_{3/2}$	5496(2)	5487	5488
$10p_{3/2}$	3662(2)	3655	3659
$11p_{3/2}$	2616(2)	2610	
$12p_{3/2}$	1962(1)	1958	

^aThe error bars were estimated based on the agreement [13] of the predicted second-order phase shifts with known quantum defects for cesium p -states.

^bValues marked as predicted in Ref. [22].